Electronic Supplementary Material (ESI) for Dalton Transactions.

$Nb_2BN_2^-$ Cluster Anions Reduce Four Carbon Dioxide Molecules: Reactivity Enhancement by Ligands

Hai-Yan Zhou,[a], Ming Wang,[a] Yong-Qi Ding,[a] Jia-Bi Ma[a]*

[a]Key Laboratory of Cluster Science of Ministry of Education, Beijing Key Laboratory of Photoelectronic/Electrophotonic Conversion Materials, School of Chemistry and Chemical Engineering, Beijing Institute of Technology, Beijing 100190, China

Corresponding Author

*Jiabi Ma, Email: *majiabi@bit.edu.cn*

Contents

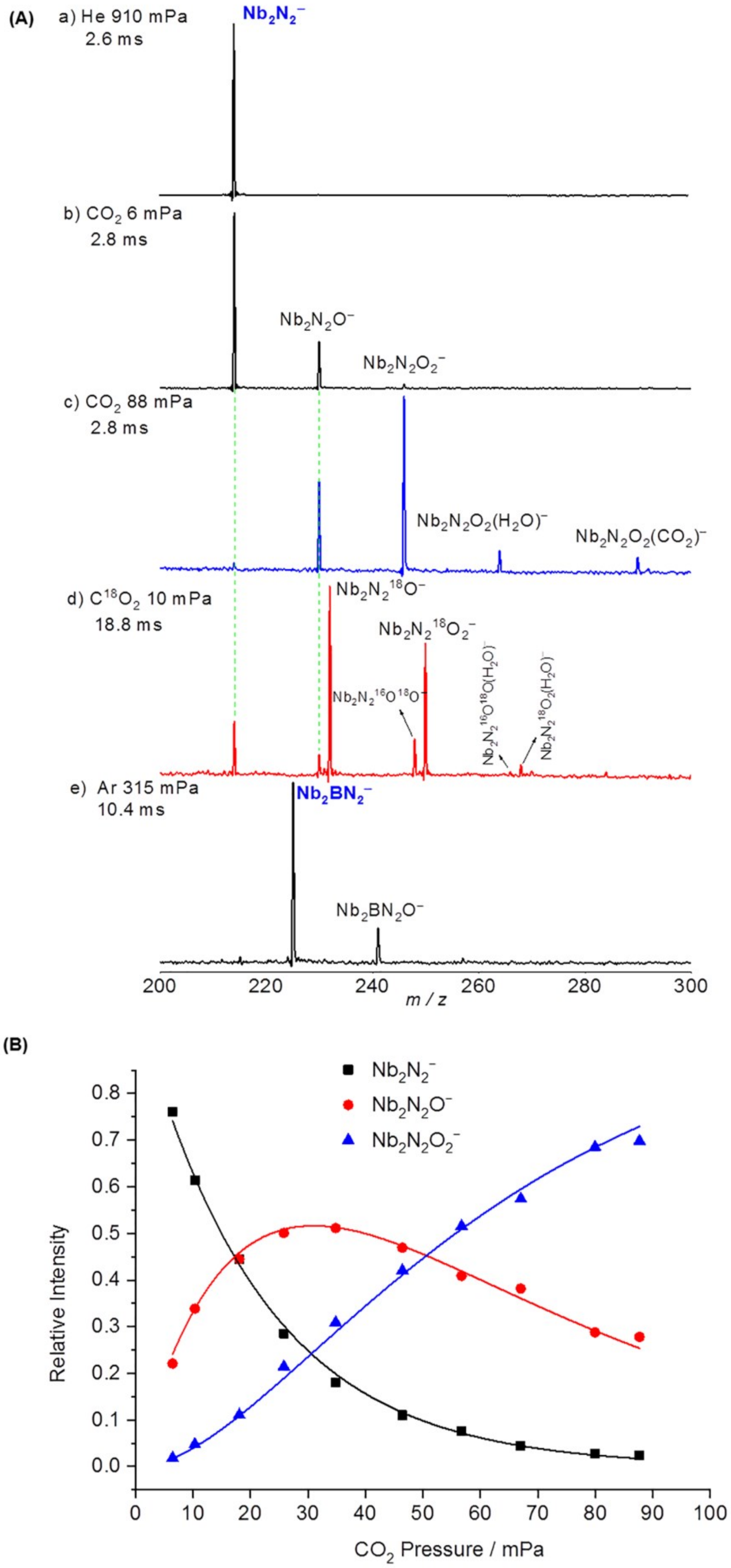

Figure S1. (A) Time-of-flight (TOF) mass spectra for the reactions of (a) mass-selected $Nb_2N_2^-$ with (b) 6 mPa CO_2 (c) 88 mPa CO_2 (d) 10 mPa $C^{18}O_2$ for 2.8 ms and (e) mass-selected $Nb_2BN_2^-$ with Ar 315mPa for 10.4 ms. The weak peaks such as $Nb_2N_2O_2(H_2O)^-$ in panel b and $Nb_2N_2{}^{16}O^{18}O(H_2O)^-$ in panel c are due to the residual water in the LIT. (B) Variations of the relative intensities of the reactant and product cations in the reaction of $Nb_2N_2^-$ and CO_2 with respect to the CO_2 pressures for 2.8 ms. The solid lines are fitted to the experimental data points by using the equations derived with the approximation of the pseudo-first-order reaction mechanism.

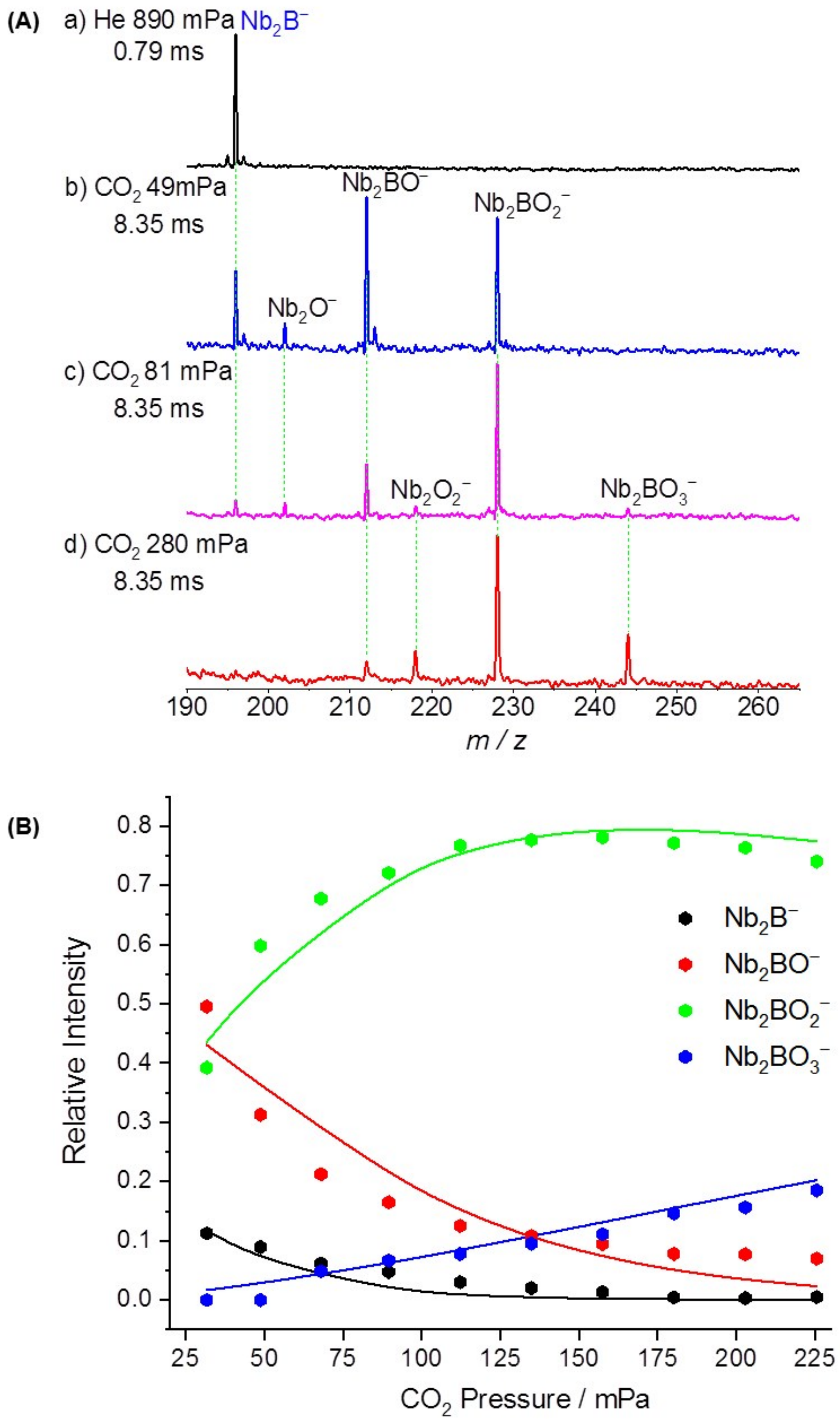

Figure S2. (A) Time-of-flight (TOF) mass spectra for the reactions of (a) mass-selected Nb_2B^- with (b) 49 mPa CO_2, (c) 81 mPa CO_2 and (d) 280 mPa CO_2 for 8.35 ms. The weak peaks such as Nb_2O^- in panel b and $Nb_2O_2^-$ in panels c,d are due to the residual water in the LIT. (B) Variations of the relative intensities of the reactant and product cations in the reaction of Nb_2B^- and CO_2 with respect to the CO_2 pressures for 8.35 ms. The solid lines are fitted to the experimental data points by using the equations derived with the approximation of the pseudo-first-order reaction mechanism.

Table S1. DFT-calculated and experimental bond dissociation energies. The values are in unit of eV.

Methods	Exp.	Nb-C	Nb-O	Nb-Nb	B-O	C-O	N-O	σ[1]
		5.897 ±0.135	7.996 ±0.260	5.286 ±0.104	8.382 ±0.217	11.16 ± 0.004	6.535 ± 0.001	
references		[1]	[2]	[3]	[2]	[4]	[5]	
Hybrid Functionals	B1B95	5.07	7.46	3.62	8.31	11.03	6.54	0.79
	B1LYP	4.92	7.38	3.66	8.12	10.70	6.35	0.85
	B3LYP	5.15	7.63	4.02	8.33	10.94	6.62	0.63
	B3P86	5.26	7.73	3.85	8.57	11.20	6.85	0.67
	B3PW91	4.98	7.45	3.39	8.38	10.95	6.56	0.89
	M05	6.22	7.57	5.22	8.07	11.02	6.39	0.27
	M052X	5.01	7.02	3.33	5.52	10.99	6.39	1.52
	PBE1PBE	4.98	7.37	3.27	8.36	10.95	6.54	0.94
	X3LYP	5.14	7.62	4.00	8.32	10.93	6.60	0.64
	M06	5.98	7.84	5.74	8.41	11.11	6.37	0.21
	M062X	5.50	7.49	3.99	5.58	11.09	6.44	1.29
	BH&HLYP	4.27	6.62	2.38	5.14	10.21	5.65	2.05
	BMK	4.44	7.03	2.34	8.55	11.24	6.57	1.40
Pure Functionals	**M06L**	**5.85**	**7.72**	**4.93**	**8.52**	**11.07**	**6.45**	**0.20**
	BPW91	5.45	8.02	4.40	8.71	11.30	7.10	0.49
	BLYP	5.66	8.23	5.17	8.60	11.23	7.12	0.29
	BP86	5.73	8.30	4.97	8.80	11.48	7.34	0.44
	BPBE	5.46	8.03	4.40	8.71	11.31	7.11	0.49
	PBE	5.74	8.27	4.85	8.88	11.53	7.36	0.47
	TPSS	5.39	7.85	4.45	8.29	10.89	6.67	0.42

[1]: $\sigma = \sqrt{\frac{\sum (x_i - x_{\text{exp}})^2}{n}}$, x_i is the DFT calculated bond dissociation energy and x_{exp} is the experimental value.

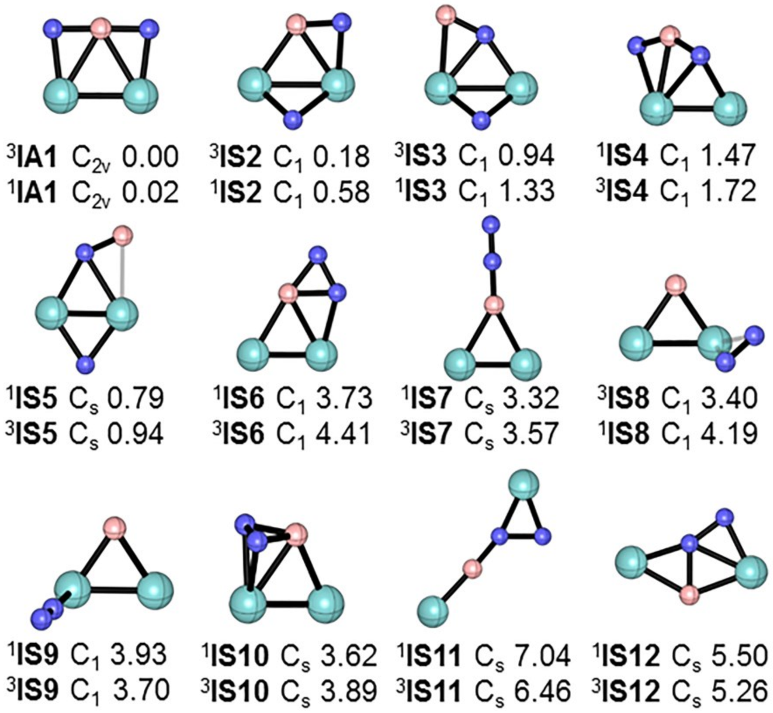

Figure S3. DFT-calculated structures and relative energies of $Nb_2BN_2^-$ at the M06L/def2-TZVPD and aug-cc-pVTZ level of theory. The point group is given under each structure. Bond lengths are given in pm. The zero-point vibration corrected energies (ΔH_{0K} in eV) of each structure are given. Superscripts denote the spin multiplicities.

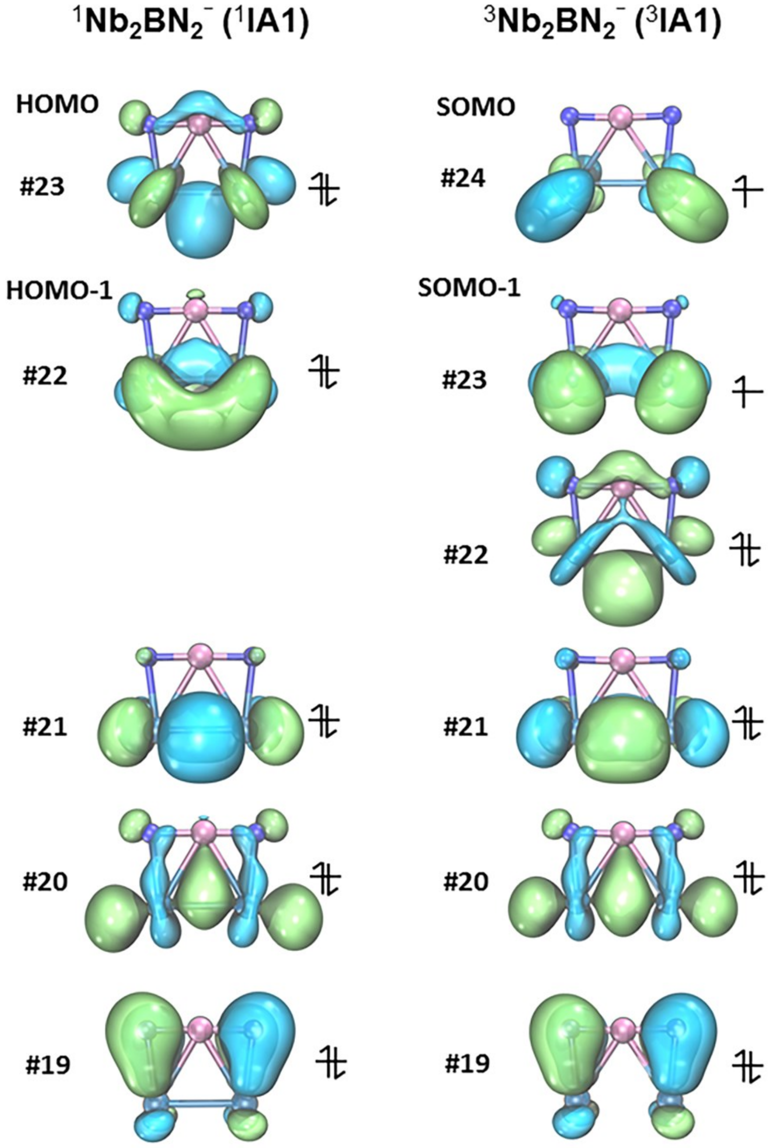

Figure S4. Schematic molecular orbital diagrams for the singlet state ^{1}**IA1** and the triplet state ^{3}**IA1**. Natural orbital partial occupation numbers are given.

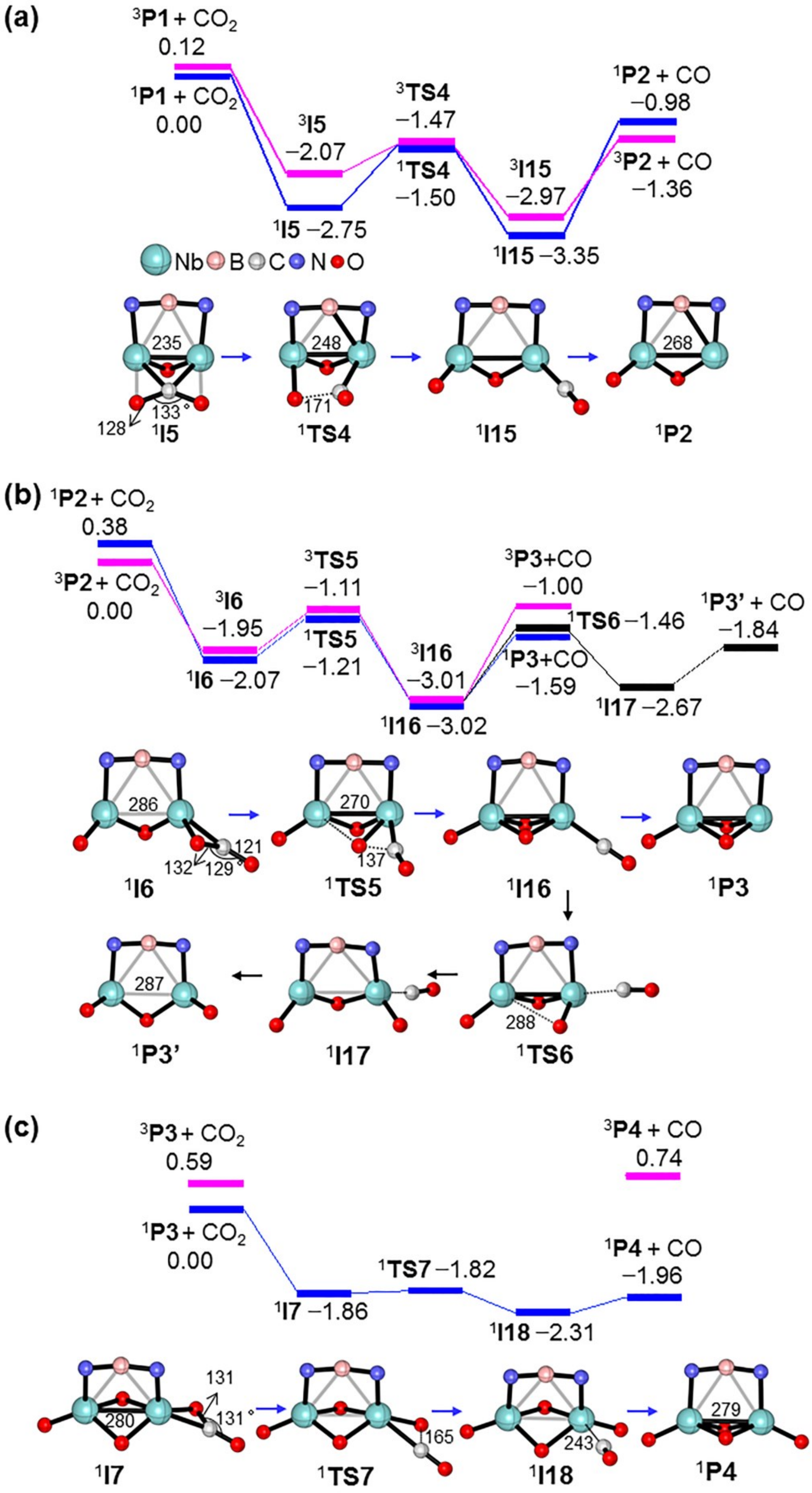
(a)
³P1 + CO₂ 0.12
¹P1 + CO₂ 0.00
³I5 −2.07
¹I5 −2.75
³TS4 −1.47
¹TS4 −1.50
³I15 −2.97
¹I15 −3.35
¹P2 + CO −0.98
³P2 + CO −1.36
Nb B C N O
235
133°
128
¹I5
248
171
¹TS4
¹I15
268
¹P2
(b)
¹P2 + CO₂ 0.38
³P2 + CO₂ 0.00
³I6 −1.95
¹I6 −2.07
³TS5 −1.11
¹TS5 −1.21
³I16 −3.01
¹I16 −3.02
³P3+CO −1.00
¹TS6 −1.46
¹P3+CO −1.59
¹I17 −2.67
¹P3' + CO −1.84
286
121
132
129°
¹I6
270
137
¹TS5
¹I16
¹P3
287
¹P3'
¹I17
288
¹TS6
(c)
³P3 + CO₂ 0.59
¹P3 + CO₂ 0.00
¹I7 −1.86
¹TS7 −1.82
¹I18 −2.31
³P4 + CO 0.74
¹P4 + CO −1.96
131
131°
280
¹I7
165
¹TS7
243
¹I18
279
¹P4

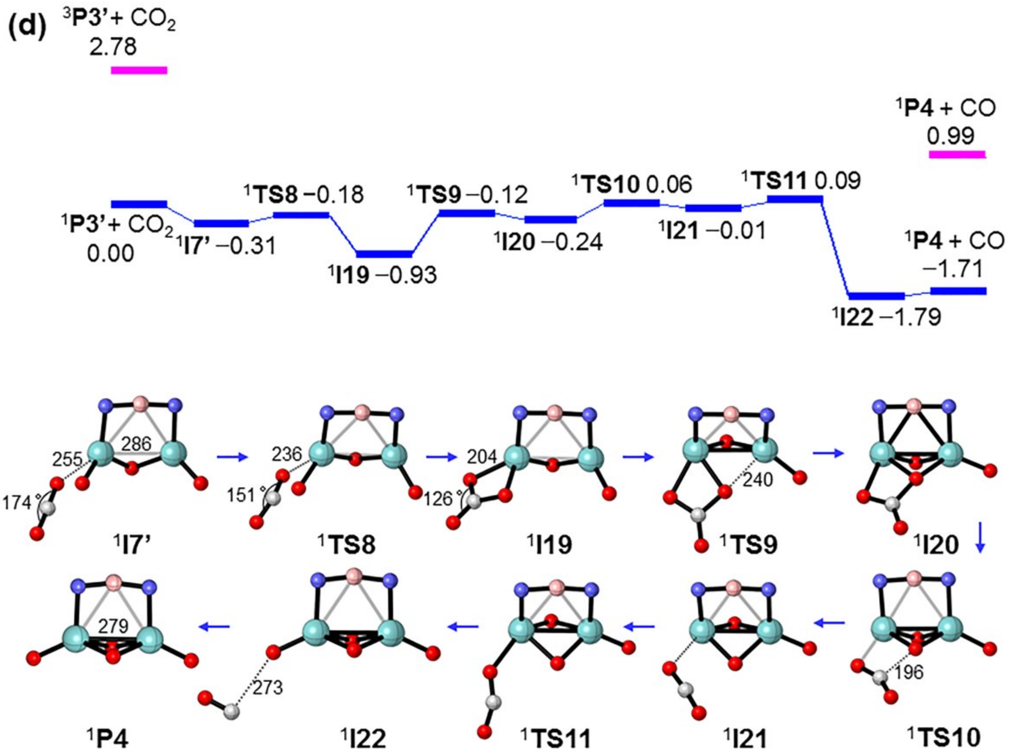

Figure S5. DFT-calculated potential energy surfaces for the reactions of (a) $Nb_2BN_2O^-$ (**P1**), (b) $Nb_2BN_2O_2^-$ (**P2**), (c) and (d) $Nb_2BN_2O_3^-$ (**P3** and **P3'**) with CO_2 at the M06L/def2-TZVPD and aug-cc-pVTZ level of theory. The zero-point vibration corrected energies (ΔH_{0K} in eV) of the reaction intermediates, transition states, and products with respect to the separated reactants are given. Superscripts denote the spin multiplicities. Bond lengths are given in pm.

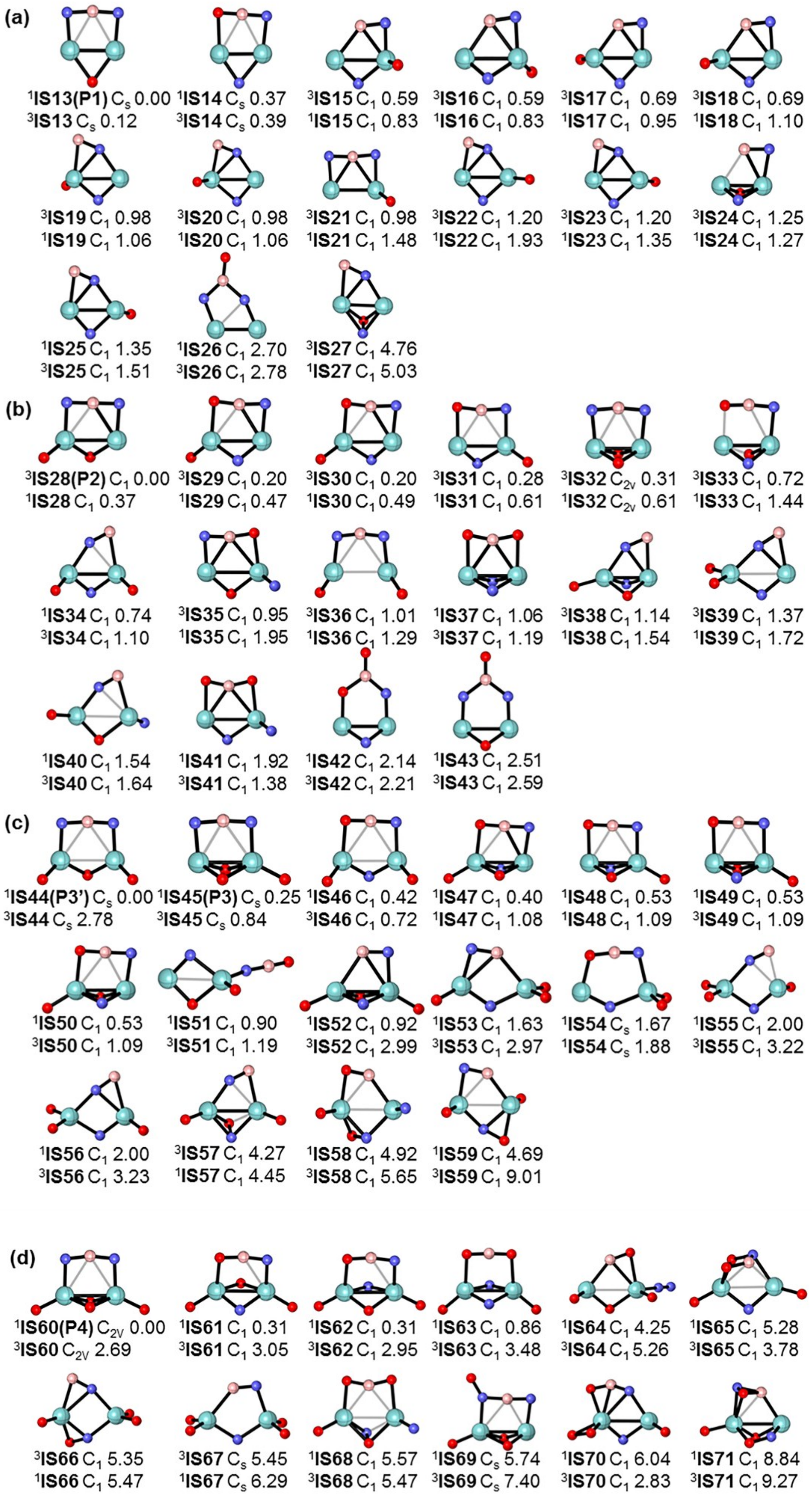

Figure S6. DFT-calculated structures and relative energies of (a) $Nb_2BN_2O^-$, (b) $Nb_2BN_2O_2^-$, (c) $Nb_2BN_2O_3^-$ and (d) $Nb_2BN_2O_4^-$ at the M06L/def2-TZVPD and aug-cc-pVTZ level of theory. The point group is given under each structure. Superscripts denote the spin multiplicities. The zero-point vibration corrected energies (ΔH_{0K} in eV) of each structure are given.

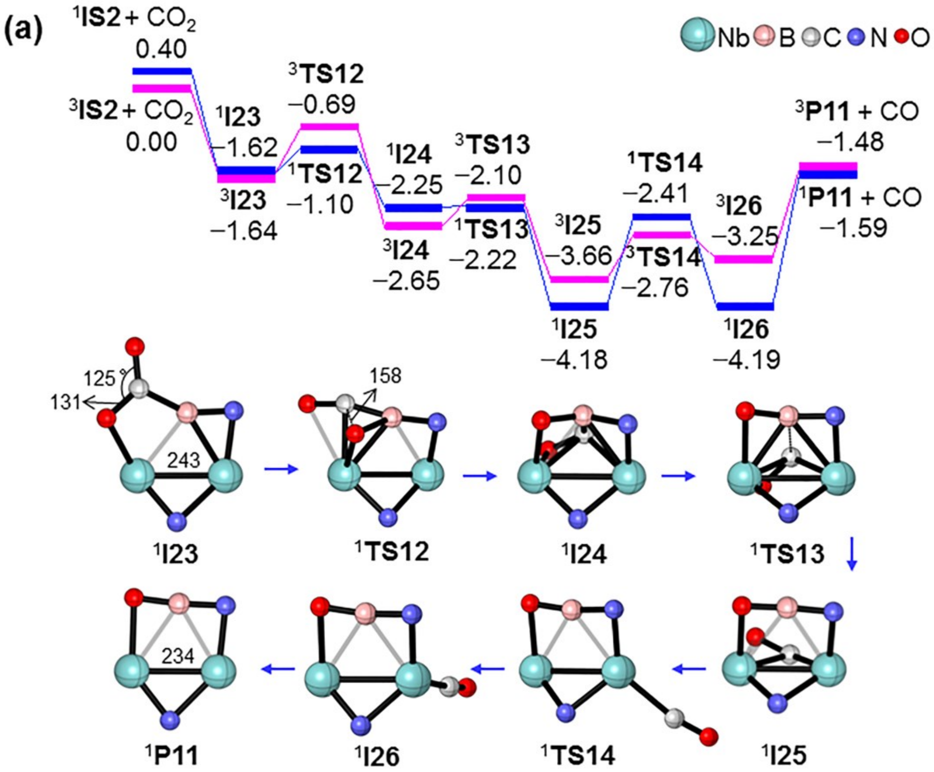
(a)
Nb B C N O
1IS2 + CO2
0.40
3IS2 + CO2
0.00
1I23
−1.62
3I23
−1.64
3TS12
−0.69
1TS12
−1.10
1I24
−2.25
3I24
−2.65
3TS13
−2.10
1TS13
−2.22
3I25
−3.66
1I25
−4.18
1TS14
−2.41
3TS14
−2.76
3I26
−3.25
1I26
−4.19
3P11 + CO
−1.48
1P11 + CO
−1.59
125°
131
243
158
1I23
1TS12
1I24
1TS13
1P11
1I26
1TS14
1I25
234

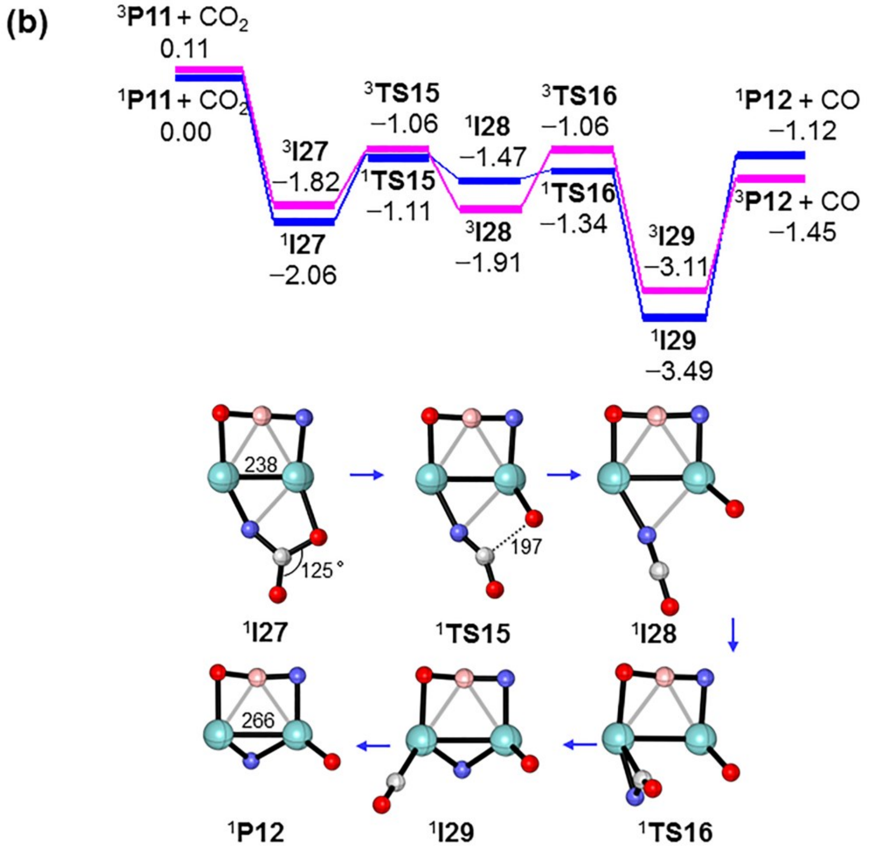
(b)
3P11 + CO2
0.11
1P11 + CO2
0.00
3I27
−1.82
1I27
−2.06
3TS15
−1.06
1TS15
−1.11
1I28
−1.47
3I28
−1.91
3TS16
−1.06
1TS16
−1.34
3I29
−3.11
1I29
−3.49
1P12 + CO
−1.12
3P12 + CO
−1.45
238
125°
197
1I27
1TS15
1I28
266
1P12
1I29
1TS16

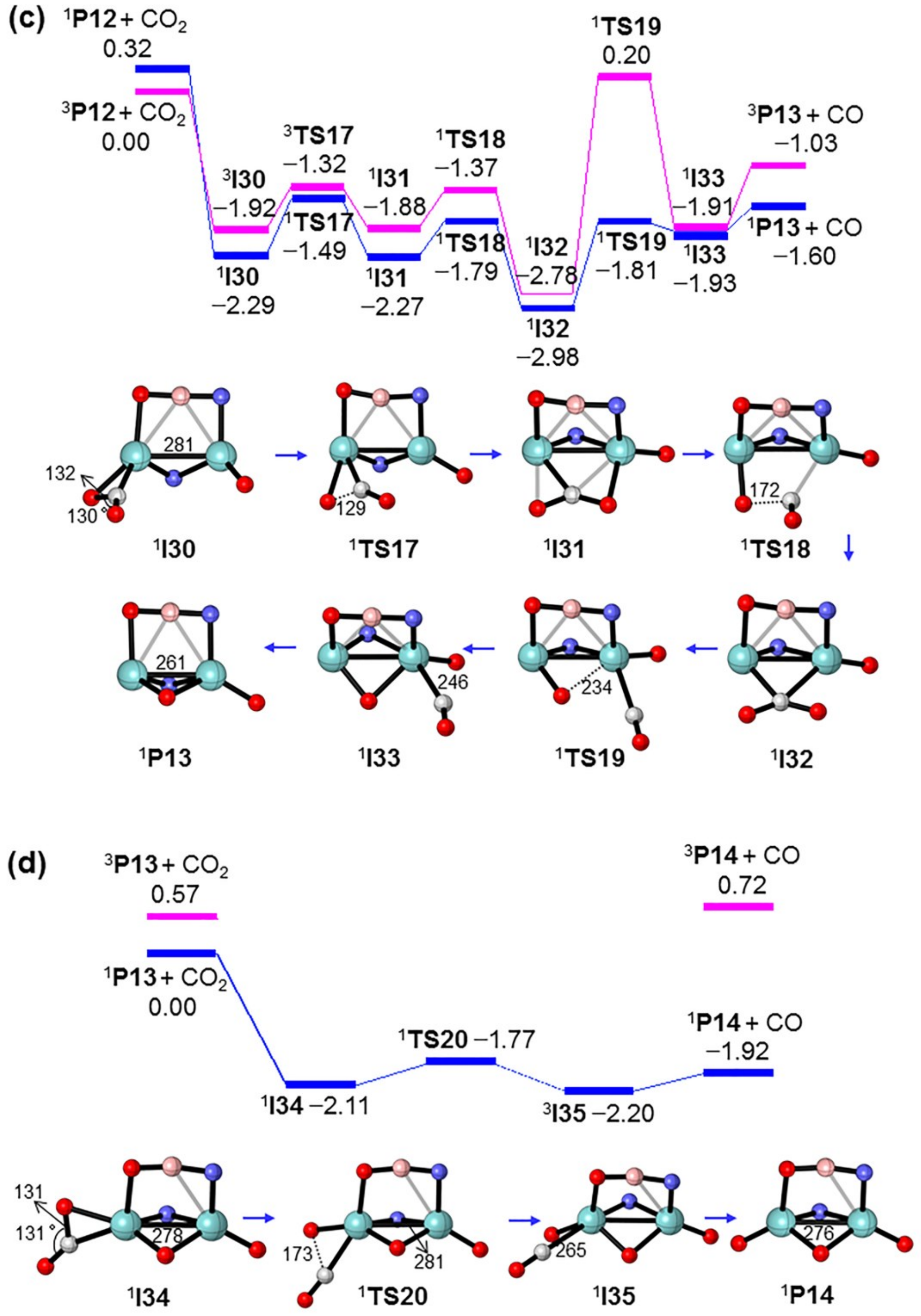

Figure S7. DFT-calculated potential energy surfaces for the reactions of the other isomer (a) $Nb_2BN_2O^-$, (b) $Nb_2BN_2O_2^-$, (c) $Nb_2BN_2O_3^-$ and (d) $Nb_2BN_2O_4^-$ with CO_2 at the M06L/def2-TZVPD and aug-cc-pVTZ level of theory. The zero-point vibration corrected energies (ΔH_{0K} in eV) of the reaction intermediates, transition states, and products with respect to the separated reactants are given. Superscripts denote the spin multiplicities. Bond lengths are given in pm.

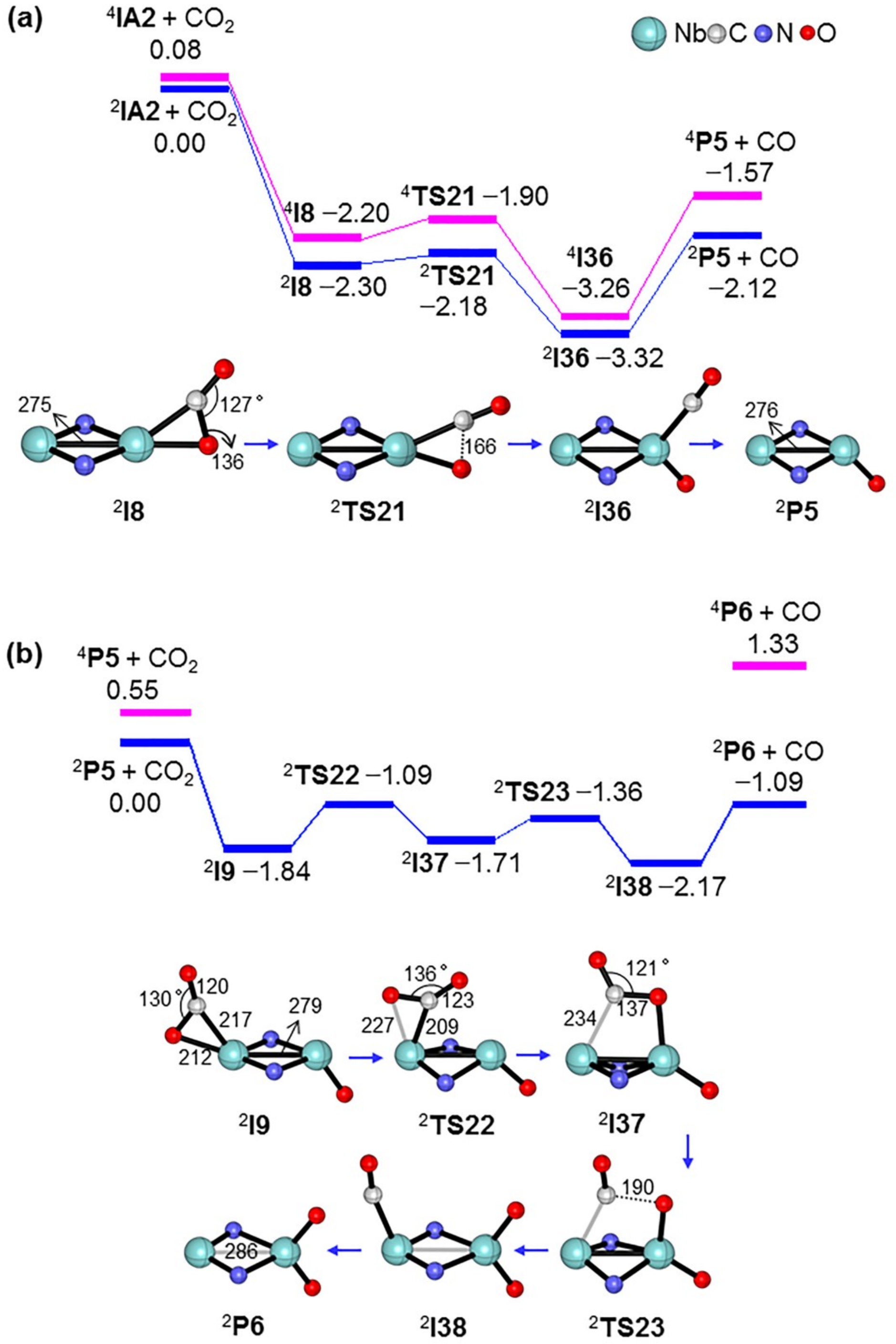

Figure S8. DFT-calculated potential energy surfaces for the reactions of (a) $Nb_2N_2^-$ and (b) $Nb_2N_2O^-$ (**P5**) with CO_2 at the M06L/def2-TZVPD and aug-cc-pVTZ level of theory. The zero-point vibration corrected energies (ΔH_{0K} in eV) of the reaction intermediates, transition states, and products with respect to the separated reactants are given. Superscripts denote the spin multiplicities. Bond lengths are given in pm.

Path I

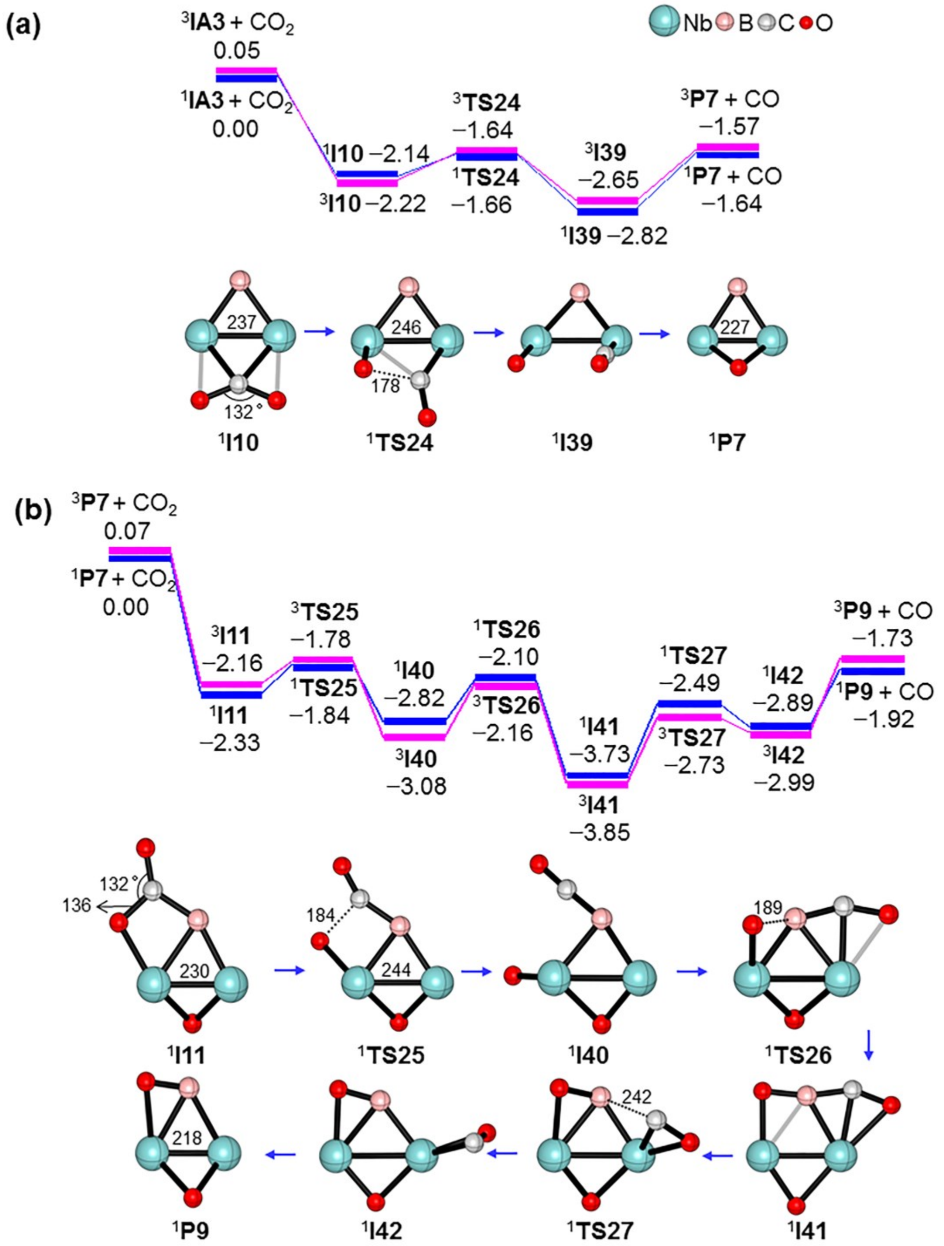

Path II

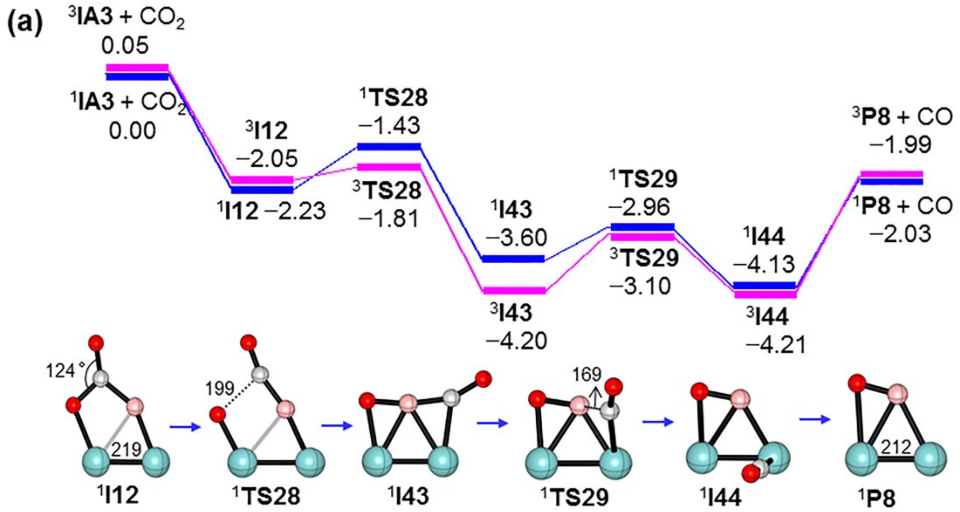

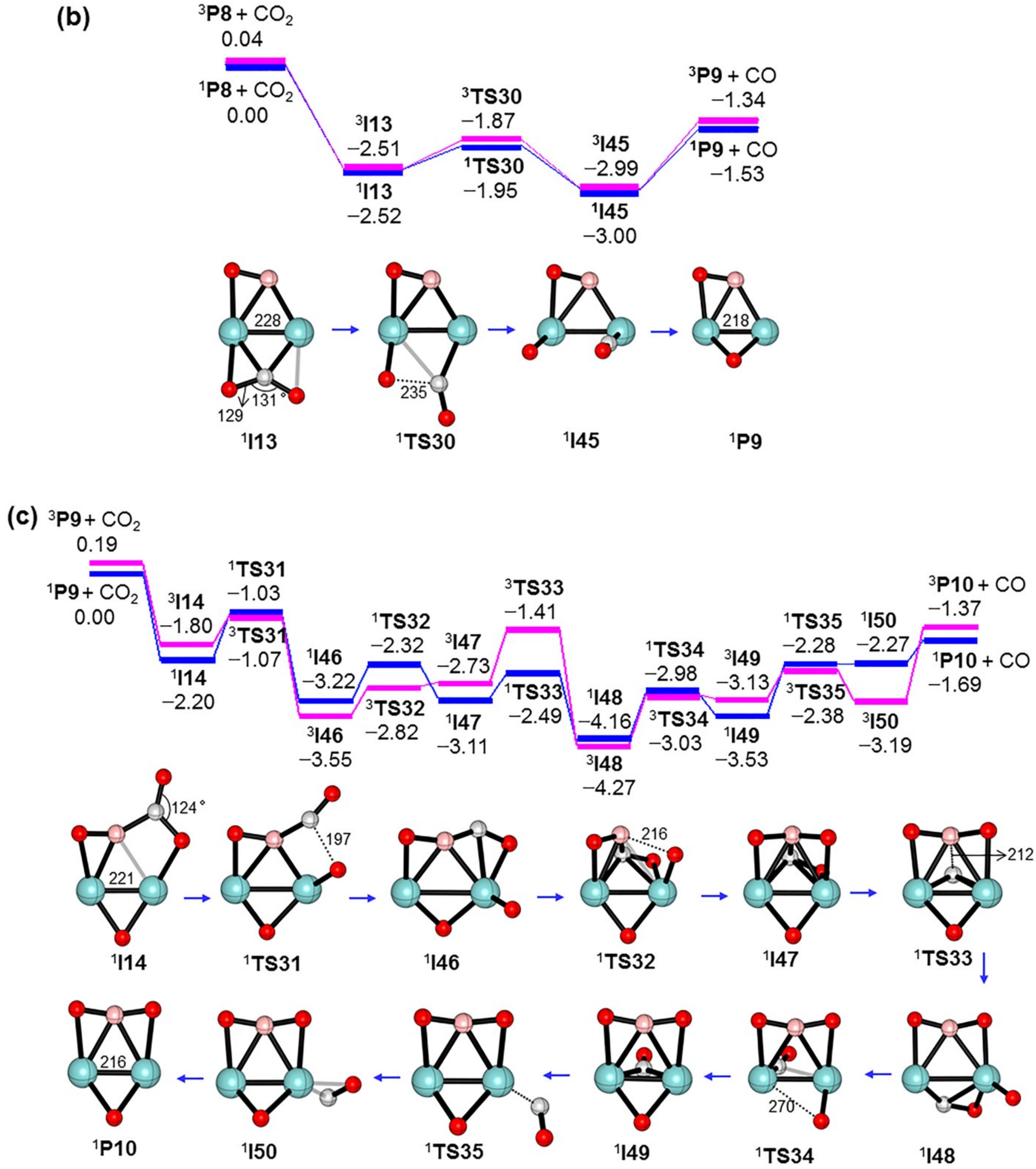

Figure S9. DFT-calculated potential energy surfaces for the reactions of (a) Nb_2B^-, (b) Nb_2BO^- (**P7** in Path I and **P8** in Path II) and (c) $Nb_2BO_2^-$ (**P9**) with CO_2 at the M06L/def2-TZVPD and aug-cc-pVTZ level of theory. The zero-point vibration corrected energies (ΔH_{0K} in eV) of the reaction intermediates, transition states, and products with respect to the separated reactants are given. Superscripts denote the spin multiplicities. Bond lengths are given in pm.

Note that in panel c, a two-state reactivity (TSR) scenario between singlet and triplet spin states is involved in the pathways of the $Nb_2BO_2^-/CO_2$ system. Considering the facts that the calculated barriers for this reaction lie below the reactant energies and the experimentally observed reaction is not very efficient, we conclude that spin-orbit coupling (SOC) constants at minimum-energy crossing points may be small.

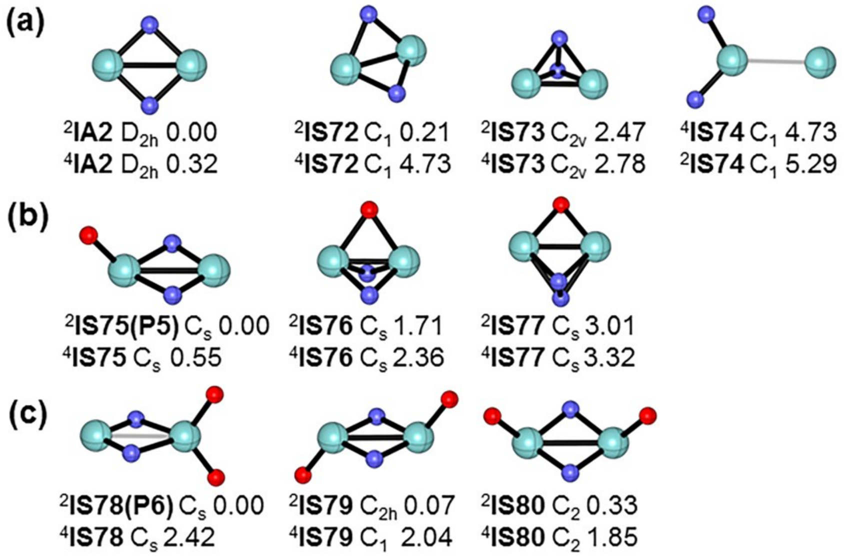

Figure S10. DFT-calculated structures and relative energies of (a) $Nb_2N_2^-$, (b) $Nb_2N_2O^-$ and (c) $Nb_2N_2O_2^-$ at the M06L/def2-TZVPD and aug-cc-pVTZ level of theory. The point group is given under each structure. Bond lengths are given in pm. Superscripts denote the spin multiplicities. The zero-point vibration corrected energies (ΔH_{0K} in eV) of each structure are given.

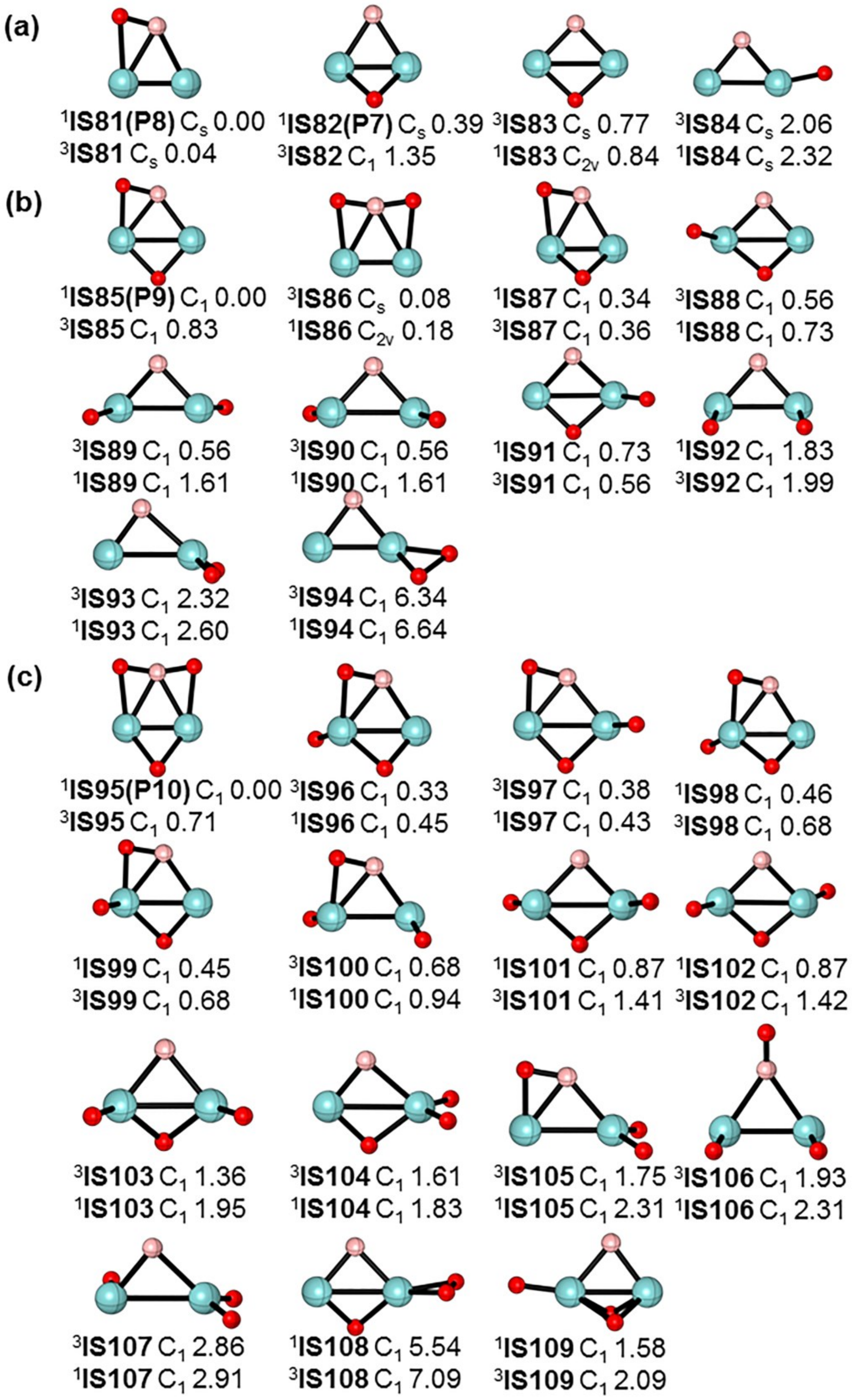

Figure S11. DFT-calculated structures and relative energies of (a) Nb_2BO^-, (b) $Nb_2BO_2^-$ and (c) $Nb_2BO_3^-$ at the M06L/def2-TZVPD and aug-cc-pVTZ level of theory. The point group is given under each structure. Bond lengths are given in pm. Superscripts denote the spin multiplicities. The zero-point vibration corrected energies (ΔH_{0K} in eV) of each structure are given.

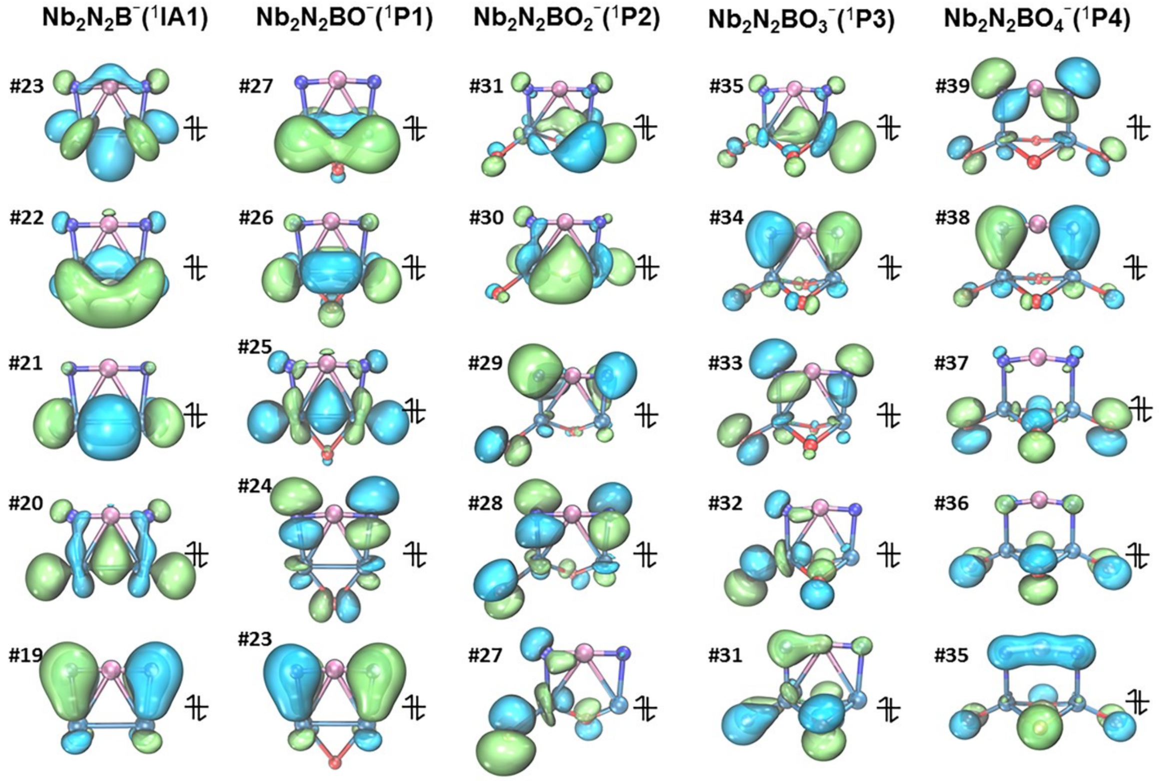

Figure S12. Schematic molecular orbital diagrams for $^1Nb_2BN_2O_{0\text{-}4}^-$. Natural orbital partial occupation numbers are given.

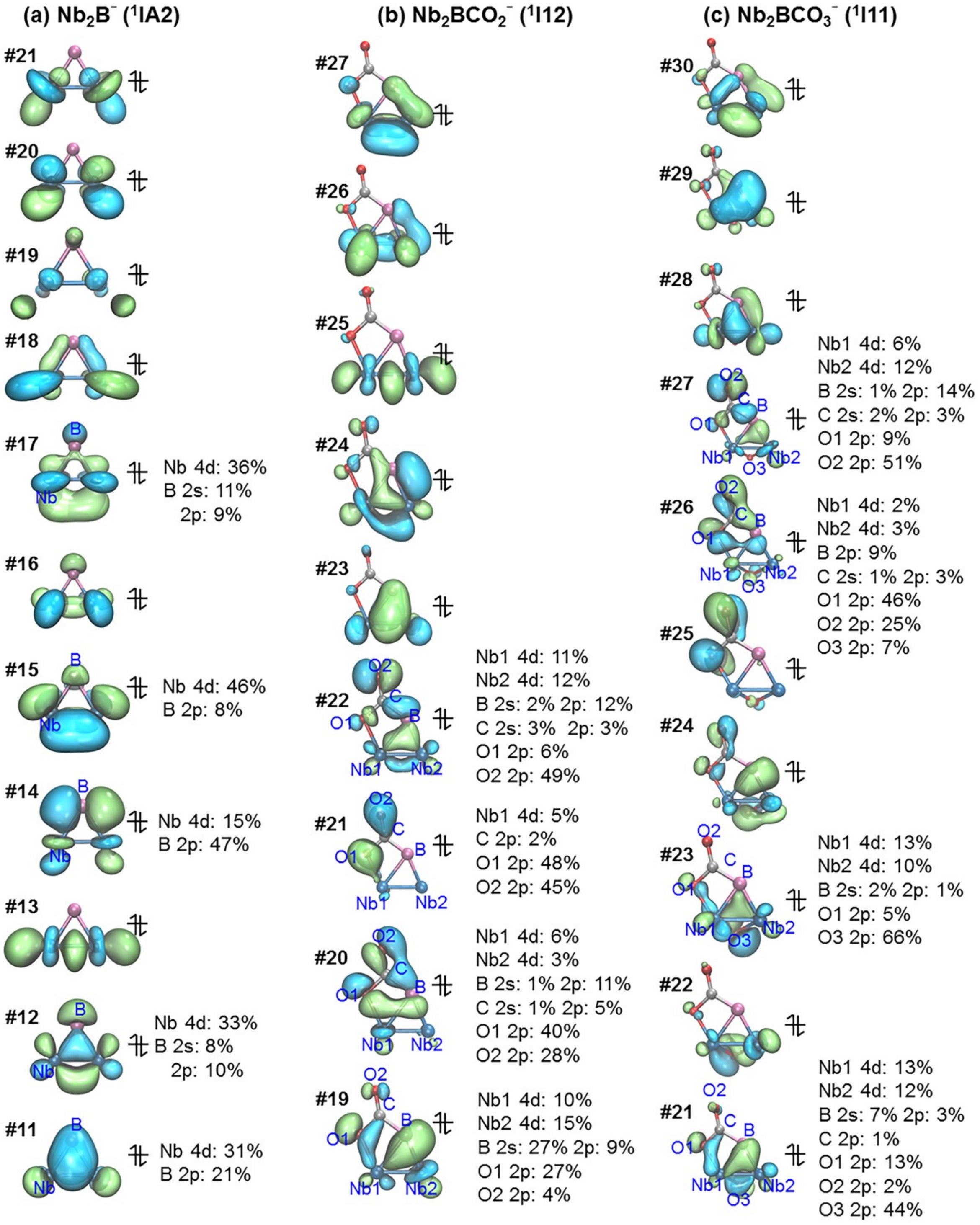

Figure S13. Schematic molecular orbital diagrams for (a) ^{1}**IA2**, (b) ^{1}**I12** and (c) ^{1}**I11.** The compositions of some key molecular orbitals are given. Natural orbital partial occupation numbers are given.

References

[1] S. K. Gupta, K. A. Gingerich, *J. Chem. Phys.* **1981**, *74*, 3584-3590.

[2] J. B. Pedley, E. M. Marshall, *J. Phys. Chem. Ref. Data.* **1983**, *12*, 967-1031.

[3] S. K. Gupta, K. A. Gingerich, *J. Chem. Phys.* **1979**, *70*, 5350-5353.

[4] A. M. Cuthill, D. J. Fabian, S. Shu-Shou-Shen, *J. Phys. Chem.* **1973**, *77*, 2008-2011.

[5] K. P. Huber, G. Herzberg, Molecular Spectra and Molecular Structure Constants of Diatomic Molecules. New York: Van Nostrand Reinhold Company, **1978**: 222-223.